Interplay of ferroelectricity and single electron tunneling

S. A. Fedorov,[1,2] A. E. Korolkov,[1,2] N. M. Chtchelkatchev,[1,3,4,5] O. G. Udalov,[3,6] and I. S. Beloborodov[3]
[1]*Department of Theoretical Physics, Moscow Institute of Physics and Technology, Moscow 141700, Russia*
[2]*P.N. Lebedev Physical Institute of the Russian Academy of Sciences, Moscow 119991, Russia*
[3]*Department of Physics and Astronomy, California State University Northridge, Northridge, California 91330, USA*
[4]*L.D. Landau Institute for Theoretical Physics, Russian Academy of Sciences, Moscow 117940, Russia*
[5]*Institute for High Pressure Physics, Russian Academy of Science, Troitsk 142190, Russia*
[6]*Institute for Physics of Microstructures, Russian Academy of Science, Nizhny Novgorod, 603950, Russia*
(Received 15 February 2014; revised manuscript received 25 March 2014; published 7 April 2014)

We investigate the interplay of ferroelectricity and quantum electron transport at the nanoscale in the regime of Coulomb blockade. Ferroelectric polarization in this case is no longer the external parameter but should be self-consistently calculated along with electron hopping probabilities leading to physical transport phenomena studied in this paper. These phenomena appear mostly due to effective screening of a grain electric field by ferroelectric environment rather than due to polarization dependent tunneling probabilities. At small bias voltages polarization can be switched by a single excess electron in the grain. In this case transport properties of a single electron transistor exhibit the instability (memory effect).

DOI: 10.1103/PhysRevB.89.155410 PACS number(s): 77.80.−e, 72.80.Tm, 77.84.Lf

Systems with ferroelectric (FE) elements attract much of the attention due to their interesting fundamental properties at the nanoscale as well as due to their possible applications in microelectronics, especially in nonvolatile memory devices, in emerging technologies of Terahertz-detecting, and in building of advanced (nano)capacitors [1–14]. In quantum junctions the ferroelectricity influences electron transport: Tunneling through the FE barriers shows giant electroresistance effect caused by the strong dependence of electron tunneling probability on the FE polarization and external bias orientations [7,15]. Here we focus on the inverse process—the influence of electron transport on ferroelectricity [2,10]. The naive guess would be that a single electron, small quantum object, can slightly influence the macroscopic effect—ferroelectricity. However, we show that this is not quite true and discuss the interplay of ferroelectricity and quantum electron transport at the nanoscale in the regime of Coulomb blockade. Polarization in this case is no longer the external parameter but should be self-consistently calculated along with electron hopping probabilities leading to physical transport phenomena studied in this paper. These phenomena appear mostly due to effective screening of a grain electric field by ferroelectric environment rather than due to polarization dependent tunneling probabilities.

Ferroelectrics (FE) are characterized by the polarization **P** whose direction and magnitude can be changed by applying an external electric field $\mathcal{E}$ larger than the ferroelectric switching field $\mathcal{E}_s$. The ground ferroelectric state of a bulk sample is usually not uniformly polarized but divided into domains to lower the electrostatic energy, like in ferromagnets [16].

At the nanoscale to influence the polarization of a (nano)ferroelectric one can apply strong enough bias to nanotips [2]: There is a well developed technique of imaging and control of domain structures in ferroelectric thin films by a tip of a scanning probe microscope, see, e.g., Refs. [2,7,10,17–19].

Here we show how ferroelectric polarization switching can be produced by placing a single excess electron at the nanograin. A charged metal particle creates a strong enough electric field, $\mathcal{E} \approx 1$ MV/cm, around it. Numerous ferroelectric (nano)materials have the same order of magnitude switching field [2,10].

We study a single electron device with electric current flowing from the source to the drain electrodes with voltages V_1 and V_2, respectively, Fig. 1. A metallic nanoparticle is placed in between these electrodes. The third gate electrode controls the effective number of electrons on the grain through the capacitive coupling. We assume that the charging energy E_c of a single grain is the leading energy scale in the problem $E_c \gg T$ with T being the temperature. The device shown in Fig. 1 is a standard single electron transistor (SET) [20–27] with one important exception: electrons tunnel through ferroelectric insulating layers.

The tunnel junctions between the nanograin and the electrodes form the capacitors with ferroelectric filling (see equivalent electric circuit Fig. 2). Typically, ferroelectric placed into the capacitor chooses polarization direction perpendicular to the electrodes. This configuration reduces electrostatic energy due to FE polarization screening by the electrodes. The direction of polarization can be switched applying the bias voltage to the capacitor. In SET the potentials of the electrodes and the gate potential are usually fixed. The grain potential ϕ can fluctuate and can be found by solving simultaneously the electrostatic and the electron transport problems. The potential ϕ depends not only on the bias voltage and capacitances, but also on the probability distribution $p(n)$ to find n electrons on the grain and on the polarization of ferroelectrics. Polarizations of ferroelectric layers in turn depend on the grain potential and $p(n)$. Thus we need to consider the self-consistent problem.

The solution of the self-consistent problem strongly depends on the relaxation parameters of the ferroelectric material: How quickly the polarizations can change (flip) during the characteristic time of charging (discharging) of SET by a single electron. Below we focus on two limiting cases when both ferroelectric layers have relaxation times much longer than a one-electron charging-discharging time and vice versa. These two cases correspond to qualitatively different behavior of FE SET.

1098-0121/2014/89(15)/155410(9) ©2014 American Physical Society

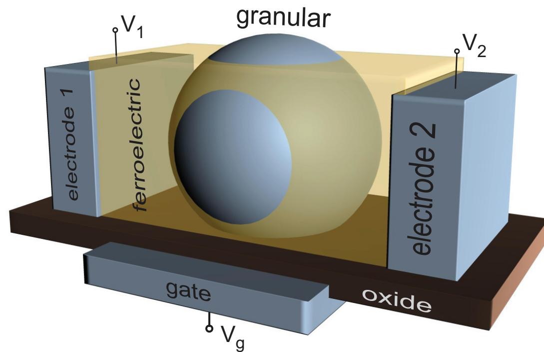

FIG. 1. (Color online) Sketch of a single electron device with ferroelectric tunnel junctions.

The case of slow FE is considered in Sec. I B. We study the dependence of FE state on bias and gate voltages and show that the Coulomb diamonds have the "fine structure" mediated by ferroelectricity that depends on the gate voltage, Fig. 3 (at large enough ferroelectric polarizations this fine structure can become comparable with the size of the diamonds). We present the plot of FE "phase diagram," Fig. 4. For large bias voltages the polarization in both capacitors are co-directed and does not affect the electron transport. At small bias voltages the polarization can be switched by a single excess electron in the grain. In this case transport properties of SET exhibit the instability (hysteresis), Fig. 3. We emphasize that this instability appears even without the hysteresis of polarization $P(\mathcal{E})$.

In Sec. I C we discuss the case of fast FE. Then the instability is absent. However, we show that the Coulomb-blockade peaks of zero-bias conductance as the function of the gate voltage [20–23] become wider and finally disappear with increasing of the FE polarizations. Such an effect appears due to strong nonlinear screening of electron charge in the grain by ferroelectrics leading to the suppression of the Coulomb blockade. In Sec. II we discuss the relation of our theory to real experimental situation.

I. SINGLE ELECTRON DEVICE WITH FERROELECTRIC TUNNEL JUNCTIONS

Below we discuss the basic properties of SET sketched in Fig. 1. The equivalent electric circuit is shown in Fig. 2. The ferroelectricity influences the properties of SET through two capacitors with FE insulating layers and results in the redistribution of charge over the surface of the nanoparticle. In

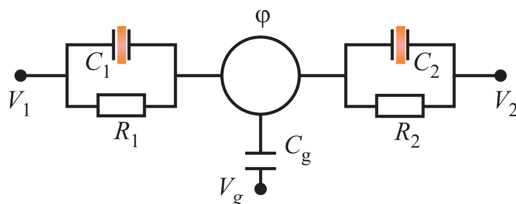

FIG. 2. (Color online) Effective circuit equivalent to the setup shown in Fig. 1. Ferroelectric insulators are highlighted by the orange color.

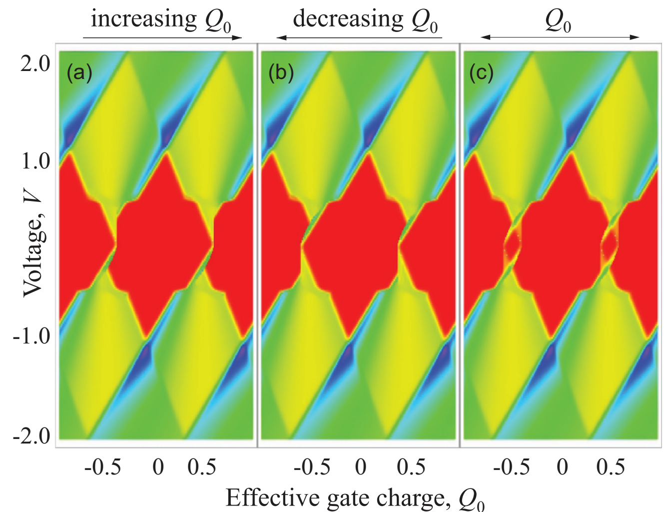

FIG. 3. (Color online) Coulomb diamonds—the conductance density plot. Here $V_{1,2} = \mp V/2$. (a) and (b) differ by the change of the evolution direction of parameter $Q_0 = -C_g V_g$. (c) Forward-backward evolution of parameter Q_0. The dimensionless temperature is $T = 0.01$ and all other parameters are similar to Fig. 5.

particular, ferroelectric with polarization $\mathbf{P}$ induces the local charge on the nanoparticle surface with the surface density $\mathbf{P}\cdot\mathbf{n}$ [16], where $\mathbf{n}$ is the normal to the surface. The excess charge on the nanograin is given by the following expression:

$$ne = \sum_i \left\{ C_i\,[\phi(n) - V_i] + \int_i d\mathbf{n}_i \cdot \mathbf{P}_i \right\}, \tag{1}$$

where n is the number of excess charges, e is the electron charge, $\phi(n)$ is the potential of the nanograin, and C_i with $i = 1,2,g$ is the capacitance. The surface integration is performed over the nanoparticle sides playing the role of the capacitor plates in Fig. 2.

We study the SET with fixed electrodes and gate potentials and find the grain potential $\phi(n)$ using Eq. (1). Following the "orthodox model" [20–23] we obtain the probabilities $p(n)$ to find n electrons on the grain. In the stationary case they satisfy the detailed balance equation

$$p(n)\Gamma_{n\to n+1} = p(n+1)\Gamma_{n+1\to n}, \tag{2}$$

where the transition rate $\Gamma_{n\to n+1}(\langle\phi\rangle)$ describes the change of grain charge from n to $n+1$ electrons, see Appendix. Calculating transition rates Γ we neglect the dependence of electron tunneling amplitudes on the FE orientation, however this effect can be easily included in our consideration. Our estimates show that consideration of polarization dependent tunneling probabilities does not destroy the effect but it rather enhances it.

The electric current can be written in terms of the transition rates as follows:

$$I = e \sum_{n=-\infty}^{\infty} p(n)\left[\Gamma^{(1)}_{n\to n-1} - \Gamma^{(1)}_{n\to n+1}\right]$$
$$= e \sum_{n=-\infty}^{\infty} p(n)\left[\Gamma^{(2)}_{n\to n+1} - \Gamma^{(2)}_{n\to n-1}\right]. \tag{3}$$

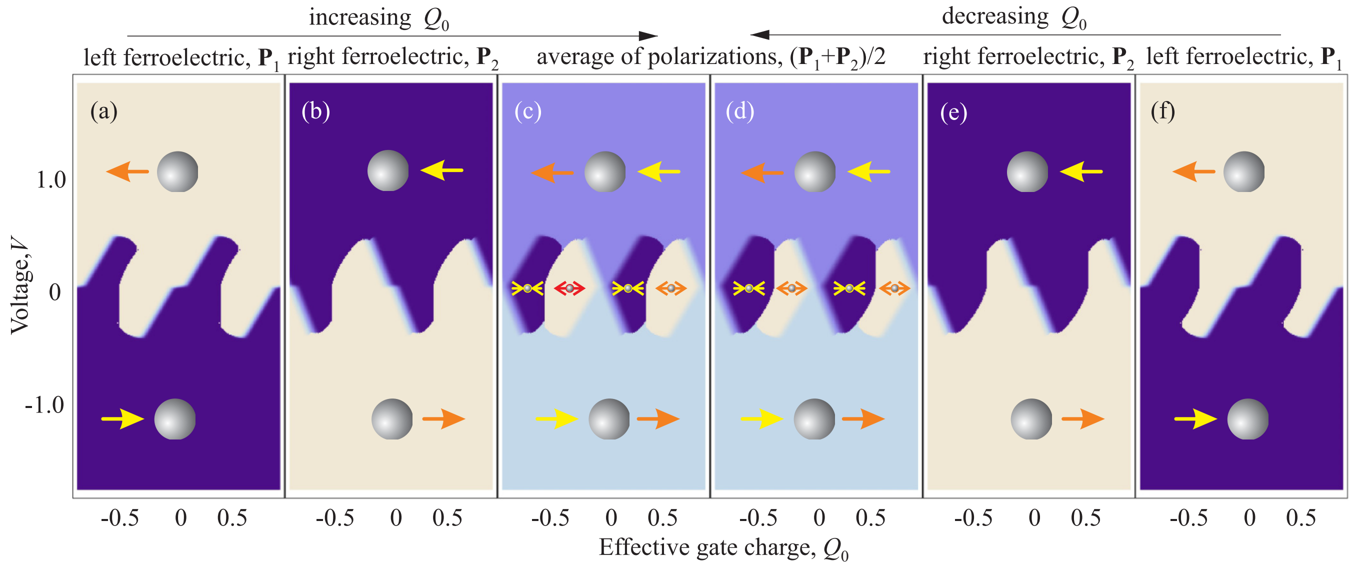

FIG. 4. (Color online) The density plot shows the "phase diagram" of the ferroelectric SET in (Q_0, V) space, where color gradients stand for polarization. The arrows show the polarizations of the left and the right ferroelectrics. (a) and (b) Ferroelectric polarizations for increasing parameter Q_0, while (e) and (f) correspond to the decreasing Q_0. (c) and (d) Arithmetical mean of the polarizations corresponding to the left and the right ferroelectrics. All parameters are similar to Fig. 3 except the parameter q_i^0: $q_1^0 = 0.03$ and $q_2^0 = 0.06$ in Eq. (7).

Here the upper index of Γ refers to the particular tunnel junction, see Appendix. Solving Eqs. (1)–(3) self-consistently we find the current I.

The polarization $\mathbf{P}$ of the FE is sensitive to the electric field and can be flipped by a strong enough field. The characteristic time scale for electron tunneling is $\tau_e = R_\Sigma C_\Sigma$, with $C_\Sigma = \sum_i C_i$ and $R_\Sigma = R_1 + R_2$ being the total capacitance and the total resistance, respectively. The characteristic time scale for polarization change $\tau_{\rm P}$ can be either larger or smaller than τ_e. Both cases are relevant for experiment and will be discussed below.

Here we consider the following model describing the electric field dependence of polarization [5,28]:

$$P(\mathcal{E}) = P^0 \tanh\left(\frac{\mathcal{E}}{\mathcal{E}_s}\right), \tag{4}$$

where $\mathcal{E}_s$ is a material dependent parameter. Similar dependence of polarization P on the capacitor voltage has the form $P(V) = P^0 \tanh(V/V_s)$, where $V_s = \mathcal{E}_s d$ and d is the distance between the electrodes of the capacitor. Equation (4) describes the saturation of P for large electric fields and it results in constant electric susceptibility $\chi_e = P^0/\mathcal{E}_s$ for small electric fields $\mathcal{E} \ll \mathcal{E}_s$. Equation (4) neglects the spontaneous polarization and the hysteresis behavior of $P(\mathcal{E})$. This simplification is valid for FE with small switching field in comparison with the field created by the charged grain, Sec. II. Below we show that even in the absence of FE hysteresis the SET conductance has history dependence. To highlight this result we neglect the FE hysteresis in our consideration. The presence of memory effect in the behavior of polarization $P(\mathcal{E})$ would add an additional hysteresis in the transport properties of SET.

A. Units for numerical calculations

We use dimensionless units in our numerical calculations: $2E_c = e^2/C_\Sigma$ is the unit of energy and temperature ($k_B = 1$). All charges are measured in units of elementary charge e, in this unit the electron has charge -1. The capacitance unit is $e^2/2E_c$, thus $C_\Sigma = 1$. We choose the bare tunnel resistance of the first tunnel junction R_1 between the left electrode and the nanograin for units of tunnel resistance, Figs. 1 and 2. Thus the unit of conductance G is $1/R_1$.

B. Mean-field approximation: Fast charging (discharging) and slow relaxation of polarization

Here we consider the limit of fast grain charging and slow relaxation of polarization $\tau_{\rm P} \gg \tau_e$. In this case the polarizations of the FE layers are defined by the *average* biases across the capacitors. The average grain potential is given by the following expression:

$$\langle\phi\rangle = \sum_{n=-\infty}^{\infty} p(n)\phi(n). \tag{5}$$

Below we show that $\langle\phi\rangle$ and $p(n)$ depend on the polarization of the FE layers that in turn depends on the average potential $\langle\phi\rangle$ leading to the self-consistent problem.

We choose $V_1 = -V/2$ and $V_2 = V/2$ for the biases applied to electrodes, solve Eq. (1) for the grain potential along with Eq. (4), and find

$$\phi(n) = \frac{e}{C_\Sigma}\left\{ne - \left[Q_0 + q_{\rm fe} + (C_1 - C_2)\frac{V}{2}\right]\right\}, \tag{6}$$

$$q_{\rm fe} = q_1^0 \tanh\left(\frac{\langle\phi\rangle + \frac{V}{2}}{V_s}\right) + q_2^0 \tanh\left(\frac{\langle\phi\rangle - \frac{V}{2}}{V_s}\right), \tag{7}$$

where $Q_0 = -C_g V_g$, $q_i^0 = P_i^0 S_i$ with $i = 1,2$, and S_i being the effective capacitance area. We notice that parameter q_i^0 is positive. Comparing Eq. (6) with the orthodox theory of SET [22,23] we find that the presence of ferroelectricity shifts the "gate charge" Q_0 by the polarization-dependent constant $q_{\rm fe}$, see Appendix.

We start our consideration with an approximate solution of Eq. (5). When the current flows through the ferroelectric SET the induced FE charge stays the same. Therefore, if we assume that the sum of the effective charges induced by the FE on the grain $q_{\rm fe}$ is known we can calculate the probability distribution of n electrons using the orthodox theory of SET.

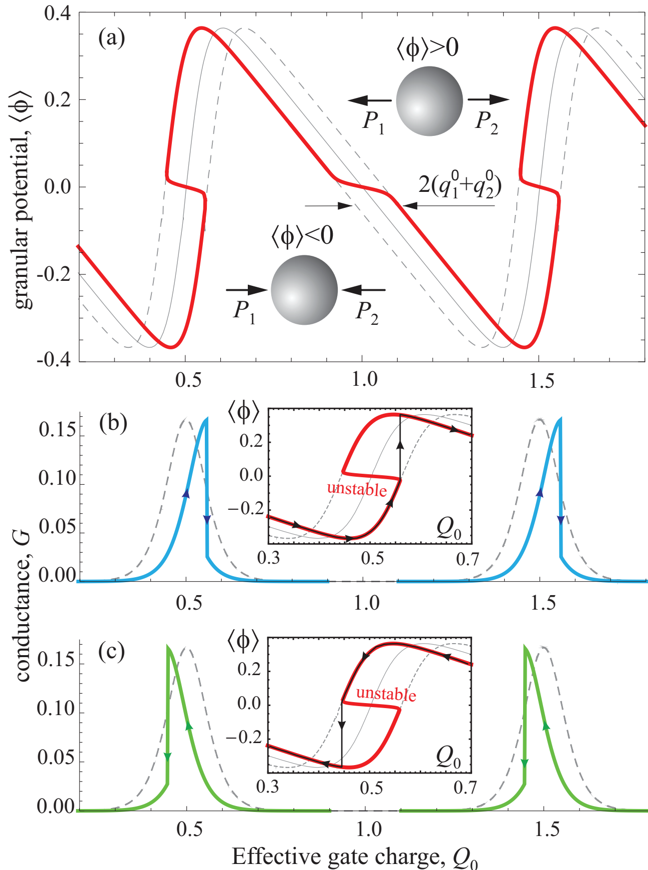

FIG. 5. (Color online) (a) Average grain potential $\langle\phi\rangle$ for voltage $V \to 0$ vs parameter Q_0. For negative potential $\langle\phi\rangle < 0$, polarizations of both ferroelectrics are directed towards the nanoparticle, while for positive potential $\langle\phi\rangle > 0$, they have the opposite direction. Plots are shown for the following set of parameters: $q_1^0 = q_2^0 = 0.03$, $T = 0.03$, $C_1 = 0.3$, $C_2 = 0.5$, $C_g = 0.2$, and $R_2 = 2R_1$. Dimensionless units are defined in Sec. I A. Almost linear branches of potential $\langle\phi\rangle$ with width $2(q_1^0 + q_2^0)$ correspond to the electric fields of both capacitors smaller than the field $\mathcal{E}_s^{(1,2)}$ in Eq. (4). The solid gray curve shows potential $\langle\phi\rangle$ for $q_1^0 = q_2^0 = 0$. (b) and (c) Conductance of ferroelectric SET vs parameter $Q_0 = -C_g V_g$. The graphs show the hysteresis effect. (b) and (c) Differ by the direction of Q_0 evolution: shown by the arrows. The gray dashed lines correspond to the conductance of SET without ferroelectricity. Insets: Black lines with arrows show the evolution of potential $\langle\phi\rangle$. The jump from one branch of $\langle\phi\rangle$ to the other corresponds to the corresponding vertical lines in the conductance curves.

The only difference between the orthodox theory and our case is the presence of an additional shift in the parameter Q_0.

We assume the following: (a) The induced FE charges are much smaller than the electron charge $|q_{\rm fe}| \ll |e|$ and (b) the bias voltage V between the first and the second electrodes of the transistor is much smaller than the charging energy $eV \ll E_c$. For $(Q_0/e - 1/2) \ll 1$ and $(Q_0 + q_{\rm fe})/e - 1/2 \ll 1$ only zero or one excess electron can be found on the grain with appreciable probability which can be obtained using the orthodox theory, Appendix A 2:

$$\frac{e\langle\phi\rangle}{E_c} = \tanh\left(\frac{E_c}{T}\frac{[\delta Q_0 + q_{\rm fe}(\langle\phi\rangle)]}{e}\right) - 2\frac{\delta Q_0 + q_{\rm fe}(\langle\phi\rangle)}{e}. \tag{8}$$

For simplicity we consider the case $\delta Q = 0$, $V = 0$, and $V_s = 0$, where Eq. (8) has a trivial solution $\langle\phi\rangle = 0$ and two nontrivial solutions

$$\langle\phi\rangle = \pm\frac{E_c}{e}\left\{\tanh\left(\frac{E_c}{T}\frac{q_1^0 + q_2^0}{e}\right) - 2\frac{q_1^0 + q_2^0}{e}\right\}. \tag{9}$$

Equation (9) agrees well with numerical results in Fig. 5 for evolution of average grain potential vs parameter Q_0. The graph is periodic in Q_0 similar to the behavior of average grain potential of SET in the absence of FE. However, there are regions in Fig. 5 where parameter Q_0 corresponds to multiple values of average potential $\langle\phi\rangle$. This behavior appears due to the reorientation of FE polarization by the average electric field inside the capacitors. Both FE orientations correspond to the same parameter Q_0. This ambiguity results in hysteresis behavior of the current.

The number of solutions in Eq. (8) depends on the system parameters V_s, E_c, and q_0. The hysteresis loop shown in Fig. 5 corresponds to the case of three solutions in Eq. (8). The criterion for hysteresis is the following, see Appendix A 3:

$$\frac{q_0}{V_s} \geqslant \frac{e^2}{E_c}\left(\frac{E_c}{T} - 2\right)^{-1}. \tag{10}$$

The width of the hysteresis loop is given by the following expression:

$$\Delta Q_0/2 \approx \frac{q_0}{V_s}\frac{E_c}{e} - \frac{eT}{E_c}. \tag{11}$$

Figure 6 shows the change of conductance hysteresis with voltage V_s. It follows that conductance discontinuity generating the hysteresis decreases with increasing voltage V_s and completely disappears above a certain critical value of V_s, see, e.g., Eq. (10). This result is natural since increasing voltage V_s produces larger FE polarizations leading to a more difficult repolarization by the external field.

The hysteresis loop is still present even if the steplike dependence of $q_{\rm fe}$ in Eq. (8) is substituted by the linear relation $q_{\rm fe} = \alpha_q\langle\phi\rangle$.

Equation (10) can be written using the dielectric susceptibility of the proper dielectric $\chi_D \approx \alpha_q d/a^2$ as follows: $\chi_D > e^2 T a^2/d E_c^2$. Thus, any dielectric with static susceptibility χ_D satisfying the above criterion and with the characteristic reaction time exceeding time τ_e will produce the hysteresis behavior in the conductivity of SET. The hysteresis in this model appears due to slow FE (or dielectric). Then the FE

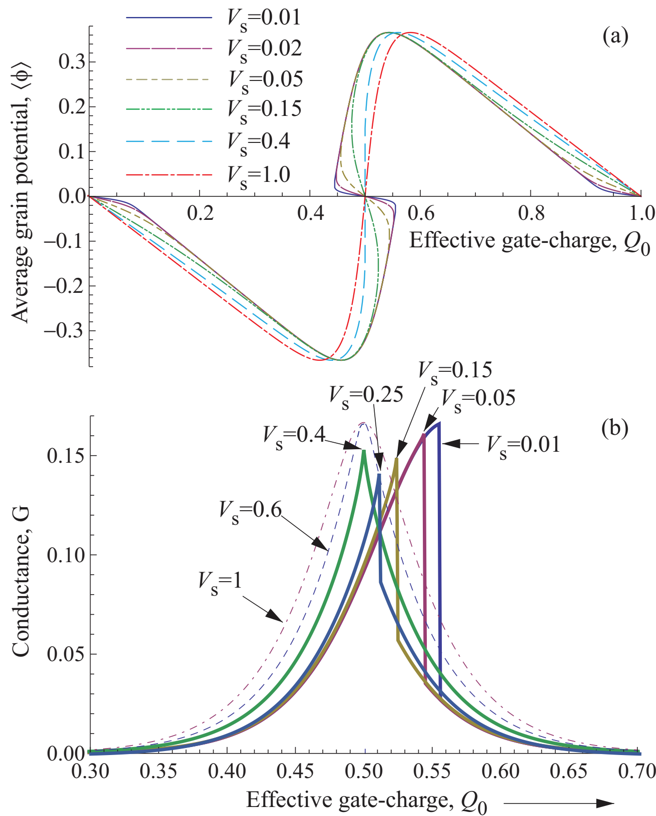

FIG. 6. (Color online) Average grain potential (a) and conductance (b) vs parameter Q_0 for different voltages V_s. All parameters (except V_s) are the same as in Fig. 5. The conductance discontinuity responsible for hysteresis becomes smaller with increasing voltage V_s and completely disappears for voltages exceeding a certain critical value of V_s.

feels only the average grain potential. We estimate parameters q_0, V_s, and the right hand side of Eq. (10) in Sec. II.

The zero voltage conductance of ferroelectric SET vs Q_0 is shown in Figs. 5(b) and 5(c). It is periodic in parameter Q_0 similar to the SET without ferroelectricity. However, the presence of ferroelectricity breaks the reflection symmetry of conductance peaks and the peaks shape depends on the direction of Q_0 change, see arrows in Figs. 5(b) and 5(c). Therefore, there is a hysteresis in the conductance behavior similar to the branching theory [29], where the points with $\frac{d\langle\phi\rangle}{dQ_0} \to \infty$ trigger the jumps between the different branches of the hysteresis loop.

Similar hysteresis behavior shows the conductance density plot in Fig. 3 with Coulomb diamonds, where Figs. 3(a) and 3(b) were obtained with forward and backward change of parameter Q_0, while Fig. 3(c) was obtained for forward-backward evolution of parameter Q_0. Ferroelectricity deforms the Coulomb diamonds: Near the half integer Q_0/e the Coulomb diamonds acquire the fine structure. However, at large enough ferroelectric polarizations this fine structure can become comparable with the size of the diamonds: The fine-structure characteristic size in the direction of Q_0 is $\approx 2[q_1^0 + q_2^0]$, for $q_1^0 + q_2^0 < 1/2$.

The hysteresis can be better understood using the energy balance consideration. The effective free energy of SET with n excess charges on the grain for zero temperature and bias voltage V has the form

$$F = E_c \min_n [n - (Q_0 + q_{\rm fe})/e]^2. \quad (12)$$

Below we use dimensionless units discussing Eq. (12). First, we compare the energies of the system for $Q_0 = 1/2$. In this case for average grain potential $\langle\phi\rangle$ according to Fig. 5 three choices are possible: $\langle\phi\rangle = 0$ and $\langle\phi\rangle = \pm\phi_0$, where $\phi_0 \approx 0.4 \gg V_s$. The first choice corresponds to $q_{\rm fe} = 0$, while two other choices to $q_{\rm fe} \approx \pm 2q^0$. The solution with $\langle\phi\rangle = 0$ corresponds to $F/E_c = 1/4$. [This value corresponds to the crossing point $Q_0 = 1/2$ of two parabolas, $(n - Q_0)^2, n = 0,1$ as functions of Q_0.] For two other cases the free energy F/E_c is smaller by $2q^0[1 - 2q_0]$. Here we choose $q^0 < 1/2$, thus the minimum in Eq. (12) corresponds to $n = 0$ or $n = 1$. The solution $\langle\phi\rangle = 0$ is physically unstable at $Q_0 = 1/2$ since it has the largest free energy. Similar consideration can be used in explaining the jumps between different branches of $\langle\phi\rangle$ in Figs. 5(b) and 5(c).

Figure 5 shows that at zero voltage one can drive the system between two states with FE layers polarized toward or backward directions with respect to the grain by changing parameter Q_0. This behavior can be understood as follows: At zero bias voltage there is no preferable direction in the SET. Contrary, a finite bias voltage results in electric field which breaks the symmetry of the problem leading to two FE polarizations in parallel.

We confirm this presenting numerical calculations of FE polarizations in the (Q_0, V) plane, Fig. 4, where the color gradients and the arrows indicate the polarizations of the left and the right ferroelectrics. Figures 4(a) and 4(b) show FE polarizations for increasing parameter Q_0 [similar to Figs. 3(a) and 5(b)], while Figs. 4(e) and 4(f) show this polarization for decreasing Q_0 [similar to Figs. 3(b) and 5(c)]. In fact, these graphs show the charges in the grain that screen the FE polarization. Figures 4(c) and 4(d) show the arithmetical mean of the polarizations corresponding to the left and to the right ferroelectrics. To distinguish the nonzero total screening charge in the parallel case we choose parameters in Fig. 4 slightly different from Figs. 3–5: $q_1^0 = 0.03$ and $q_2^0 = 0.06$.

Figure 7 shows the evolution of average grain potential $\langle\phi\rangle$ for $q_1^0 = q_2^0 = q^0$. There are several branches in the behavior of $\langle\phi\rangle$ depending on the ratio $\langle\phi\rangle/V_s$. The peaks correspond to the first branch. The nearly linear segments of $\langle\phi\rangle$ with the maximum much smaller than the peak height correspond to the second branch. Figures 7(a)–7(c) shows that the peaks of $\langle\phi\rangle$ are periodic over q^0 with the period of 0.5 ($|e|$). The shift of $\langle\phi\rangle$ peaks at $q^0 > 0$ relative to the case $q^0 = 0$ is $q_1^0 + q_2^0 = 2q^0$. The terms with $q_i^0, i = 1,2$ enter the expression for potential $\langle\phi\rangle$ similar to the shift renormalization of parameter Q_0. Figures 7(a)–7(f) show that the second branch of potential $\langle\phi\rangle$ is strongly nonperiodic.

C. Fast ferroelectric: Polarization follows charging-discharging events

Now we consider the opposite case of fast polarization following the charging-discharging process $\tau_{\rm P} \lesssim \tau_e$. In this limit the polarization P depends on the instant electric field $\mathcal{E}(n)$ instead of the average electric field $\langle\mathcal{E}\rangle$ as it was discussed

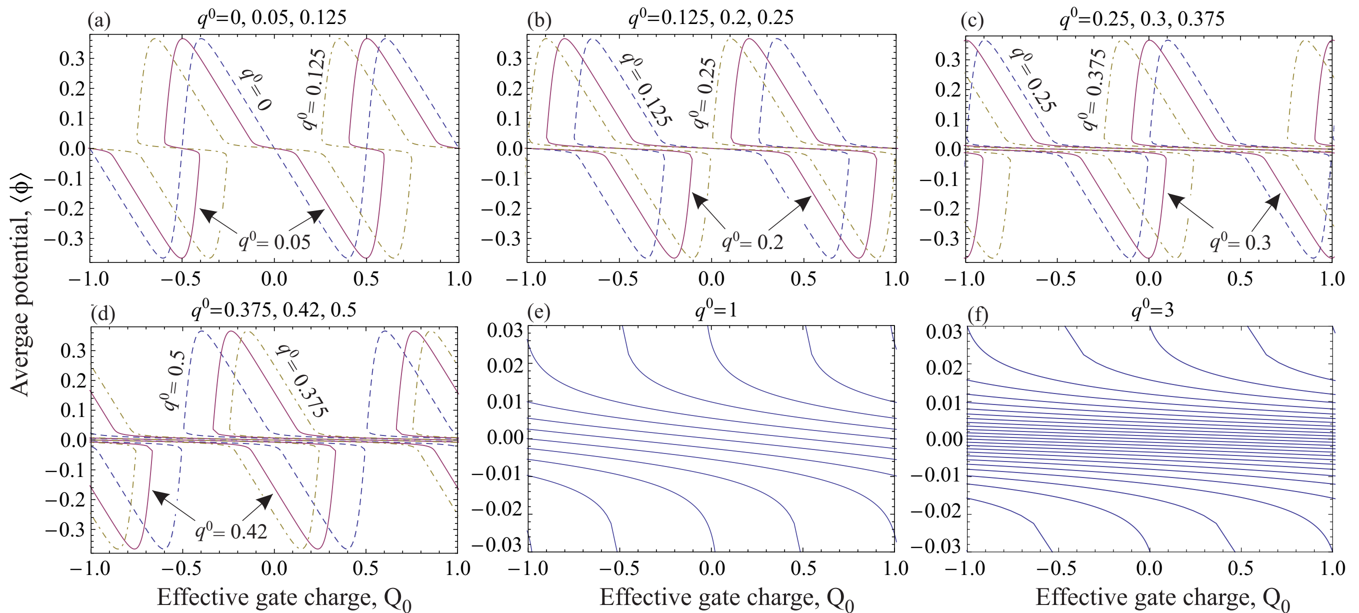

FIG. 7. (Color online) Dependence of average grain potential $\langle\phi\rangle$ on parameter $q_1^0 = q_2^0 = q^0$. (a)–(f) Oscillations of potential $\langle\phi\rangle$ in parameter q^0. The shift of potential $\langle\phi\rangle$ peaks induced by the parameter q^0 relative to the case $q^0 = 0$ is $q_1^0 + q_2^0 = 2q^0$. There are two domains of q^0 (within the first period) that produce qualitatively different relative positions of $\langle\phi\rangle$ peaks: (a)–(c) For $0 < q^0 < 1/8$ and $1/4 < q^0 < 3/8$; and (b)–(d) for $1/8 < q^0 < 1/4$ and $3/8 < q^0 < 1/2$. As follows from (e) and (f) the small-scale branch of $\langle\phi\rangle$ is nonperiodic in parameter q_0, but it is periodic in Q_0.

before. Here we replace Q_0 in the orthodox theory by $Q_s = Q_0 + q_1^0 \tanh(\frac{\phi(n)+V/2}{V_s}) + q_2^0 \tanh(\frac{\phi(n)-V/2}{V_s})$, Appendix. With this replacement Eqs. (6) and (7) remain valid with substitution of potential $\phi(n)$ instead of average potential $\langle\phi\rangle$ in Eq. (6).

The conductance behavior is shown in Fig. 8. Ferroelectricity preserves periodicity over the parameter Q_0 similar to the mean-field theory discussed in Sec. I B. However, in this limit the hysteresis is absent while the broadening of the conductance peaks, Figs. 8(a) and 8(b), and the reduction of the peaks amplitude with increasing q^0 are present, Figs. 8(c) and 8(d).

In orthodox theory the conductance of SET in the absence of ferroelectricity and at low temperatures $T \ll E_c$ follows the following relation:

$$G(\delta Q_0) = \frac{1}{2}\frac{1}{R_1 + R_2}\frac{e\,\delta Q_0/C_\Sigma T}{\sinh(e\,\delta Q_0/C_\Sigma T)}, \qquad (13)$$

where $\delta Q_0 = \min_k[Q_0 - (2k+1)\frac{e}{2}] \ll e$ is the deviation from the degeneracy point. The width of conductance peaks defines the temperature-parameter T/E_c.

For FE the degeneracy points do not follow exactly the half integer Q_0/e. Above it was shown that FE polarization redefines $Q_0 \to Q_s$ where parameter Q_s depends on the polarization and the excess charge number n. Therefore, the conductance peak in Figs. 8(a) and 8(b) has the width $(q_1^0 + q_2^0)/2$ and consists of many shifted conductance peaks (13). Thus the width of the peak plato in Fig. 8(b) is approximately $(q_1^0 + q_2^0)/2 = |e|/3$. Similar arguments explain the reduction of the conductance peaks amplitude with increasing parameter q^0 in Figs. 8(c) and 8(d).

The question about the average direction of polarizations can be investigated similar to the previous section. The results are similar, but in this case the hysteresis is absent.

At large V_s performing the linear expansion in electric field/voltage in Eqs. (4)–(6) we reproduce the result of orthodox theory for potential $\phi(n)$ with renormalized capacitances $C_i \to C_i + q_i^0/V_s^{(i)}$. Therefore, for zero-field differential dielectric susceptibility of the capacitor i we find $\epsilon^{(i)} = 1 + q_i^0/C_i V_s^{(i)}$.

II. DISCUSSION

A. Ferroelectric model

Ferroelecric SET consists of nanosized charged metallic grain embedded in a ferroelectric confined by the metallic leads, Fig. 9(a). The thickness of FE layer between the grain and the leads is a few nanometers. It is known that even for such a thin FE film the continuum theories of ferroelectricity are valid [2,30]. To determine the state of FE under the influence of the charged grain one needs to solve the inhomogeneous Landau-Ginzburg-Devonshire (LGD) equation [31]. This question appears frequently in problems dealing with local modification of FE properties by the tip of the scanning probe microscope [10]. We assume that domain wall thickness l_d in FE is less than the grain size $l_d \ll a$ [7,10]. The grain influences only the FE region between its surface and the leads, Fig. 9(b). Inside this region polarization is homogeneous and depends on the grain state. Outside this region the FE state does not depend on the grain charge. The side regions do not affect the electron transport [32]. With these assumptions the homogeneous LGD theory is valid for the description of FE behavior.

The FE material can be placed not only between the grain and the leads but also between the grain and the gate electrode, Figs. 9(c) and 9(d). In this case the FE layer does not have any metallic inclusion and can be made as a rather thick film.

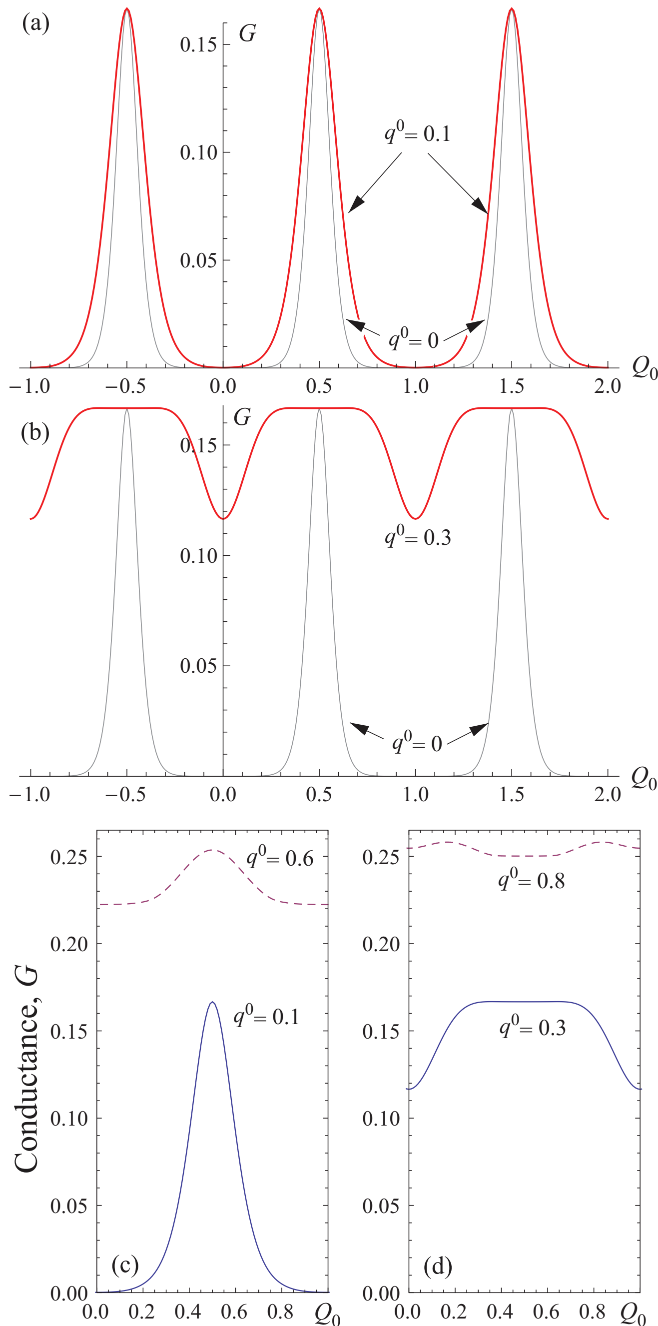

FIG. 8. (Color online) (a) and (b) Broadening of conductance peaks due to ferroelectricity: Red graph in (a) corresponds to $q_1^0 = q_2^0 = 0.1$, while in (b) $q_1^0 = q_2^0 = 0.3$. The gray graphs show the peaks for $q_1^0 = q_2^0 = 0$. (c) and (d) Reduction of the peaks amplitude with increasing q^0. The step of the q^0 increase is 0.5 similar to the "period" in Fig. 7. For plots (a)–(d) we use the following set of parameters: $T = 0.03$, $C_1 = 0.3$, $C_2 = 0.5$, $C_g = 0.2$, and $R_2 = 2R_1$, like in Fig. 5.

Such a geometry is relevant for experiment and allows us to avoid problems with the influence of grain shape on the FE polarization. The transport equations for such SET are similar to the transport equation written above. For example, in Eq. (7) one should use $q_{\rm fe} = q^0 \tanh(\frac{\langle\phi\rangle - V_g}{V_s})$, with q^0 being related to the FE between the gate and the grain.

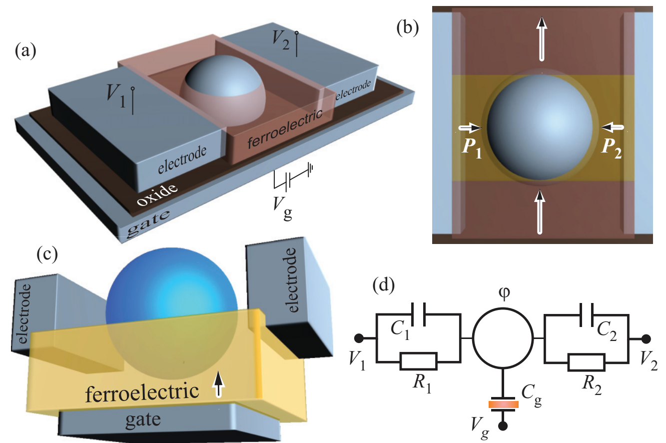

FIG. 9. (Color online) (a) Possible experimental setup with nanograin placed in a bulk ferroelectric material. (b) Top view: In the bottleneck between the electrodes and the grain, highlighted by the orange color, the ferroelectric layer is thin (quasi-two-dimensional) with polarization being unbind from the bulk ferroelectric. (c) Different geometry: Ferroelectric placed between the grain and the gate. In this case there is no restriction on the thickness of the layer: For SET no tunneling is required between the gate and the grain. (d) The equivalent electrical scheme of the SET device shown in (c).

The memory effect (hysteresis) in ferroelectric SET can be used for computer memory cell with the measurement of the zero-bias conductance being the reading operation while the application of the gate voltage being the writing operation. Such a memory cell will be discussed in the forthcoming publication.

B. Evaluation of parameters

In this section we discuss important physical parameters of FE SET such as FE and SET time scales, electric field due to metallic grain, the FE switching field, and the FE saturation polarization. These parameters define the physical behavior of FE SET.

In the previous sections we discuss two limits: (i) slow ($\tau_e < \tau_{\rm P}$) and (ii) fast ($\tau_e > \tau_{\rm P}$) ferroelectric. Estimates show that the characteristic time $\tau_e = R_\Sigma C_\Sigma$ varies in a rather large range from dozens of nanoseconds to picoseconds. This time is controlled by the system geometry and materials. The distance between the grain and the leads controls the resistivity of the SET R_Σ, the dielectric properties of the FE material, and the capacitance of the SET C_Σ. The FE switching time $\tau_{\rm P}$ depends on the material and can be in the range of 10^{-6} s [33] to a few nanoseconds [34]. Therefore, both limits are relevant for experiment. SET with changing energy $E_c \sim 300$ K have small capacitance $\lesssim 10^{-17}$ F leading to $\tau_e \ll \tau_{\rm P}$.

Discussing two limits we neglect the hysteresis loop of FE material (and thus the spontaneous polarization). This assumption is valid for large electric field created by a single electron in a grain in comparison with the FE switching field $\mathcal{E}_{\rm el} \gg \mathcal{E}_s$. This is typical for a number of FE including Li-doped ZnO [35], $Pb(In_{1/2}Nb_{1/2})_{1-x}Ti_xO_3$ [36], $[PbMg_{1/3}Nb_{2/3}O_3)_x(PbTi)_3]_{1-x}$ [37], PZT [38], etc. The presence of the hysteresis loop leads to a more complicated picture of electron transport in FE SET with the interplay of

FE hysteresis loop and the hysteresis appearing due to the interaction of FE with the grain, Sec. I B. In the opposite limit, $\mathcal{E}_{\rm el} \ll \mathcal{E}_s$, the polarization becomes an external parameter as in the ordinary FE tunnel junctions.

The magnitude of FE saturation polarization strongly affects the electron transport for fast ferroelectrics, $\tau_e > \tau_{\rm P}$. If induced charge due to FE exceeds one electron charge the Coulomb blockade is suppressed leading to the conductivity independent of the gate voltage. In this case the FE completely screens the electric field of an electron on the grain. To observe the conductivity peaks in Fig. 8 the FE environment should generate the charge smaller than one electron ($q_1^0 + q_2^0 < |e|$). Typical ferroelectrics, such as P(VDF-TrFE), PZT, $[\mathrm{PbMg}_{1/3}\mathrm{Nb}_{2/3}\mathrm{O}_3)_x(\mathrm{PbTi})_3]_{1-x}$, have bulk polarization about $P = 1\, e/\mathrm{nm}^2$ leading to $q_i^0 \gg |e|, i = 1,2$ for a few nanometer size grain. However, decreasing the thickness of FE film reduces its polarization [39]. For example, drastic polarization reduction from 1.5 to 0 e/nm is predicted for $BaTiO_3$ when the thickness of the $BaTiO_3$ film decreases from 15 to 3 nm [40]. Suppressing of polarization with decreasing of FE thickness was observed in P(VDF-TrFE) films [41].

For slow FE, Eq. (10) separates two regimes of FE SET with finite and zero hysteresis conductivity voltage dependencies. For estimates we write voltage V_s using FE switching field $V_s = d\mathcal{E}_s$ and the charge q^0 (we drop index i) using the FE polarization $q^0 \approx Pa^2$. For $P \approx 0.05$ e/nm [35], $d \approx 2$ nm, $a \approx 3$ nm, and temperature $T \approx 100$ K we find the criterion for the appearance of hysteresis $\mathcal{E}_s < 10$ MV/cm. This criterion is valid for almost all ferroelectrics. In addition, we note that in the case of slow FE the condition ($q_1^0 + q_2^0 < |e|/2$) results in simple hysteresis behavior of the system, its violation makes the behavior more complicated, but does not affect the existence of hysteresis.

III. CONCLUSION

We investigated the electron transport in a single electron device with ferroelectric active layers. We showed that there is an interplay of ferroelectricity and single electron tunneling. We distinguish two different cases of slow and fast ferroelectric. In the first case the gate voltage dependent conductance shows the instability related to the spontaneous polarization inversion of ferroelectric polarizations. We show that similar instability may also show SET with slow dielectric. At small bias voltages the polarization can be switched by a single excess electron in the grain. In the case of fast ferroelectric instability is absent. However, we show that the Coulomb-blockade peaks of zero-bias conductance as the function of the gate voltage become wider and finally disappear with increasing of the FE polarizations. Such an effect appears due to strong nonlinear screening of an electron charge in the grain by ferroelectrics leading to the suppression of the Coulomb blockade. Finally, we show that our results could be observed experimentally.

ACKNOWLEDGMENTS

N.C. was partly supported by RFBR No. 13-02-00579, the Grant of President of Russian Federation for support of Leading Scientific Schools, RAS presidium and Russian Federal Government programs. I.B. was supported by NSF under Cooperative Agreement Award EEC-1160504, NSF Award DMR-1158666, and NSF PREM Award.

APPENDIX: ORTHODOX THEORY OF FERROELECTRIC SINGLE ELECTRON TRANSISTOR

1. Main equations

Below we outline the main steps that help us to understand our results in the presence of ferroelectricity using the language of orthodox theory.

In orthodox theory the rate describing the change of grain charge from n to $n+1$ electrons through the first tunnel barrier, the left one in Fig. 2(a), is

$$\Gamma^{(1)}_{n\to n\pm 1} = \frac{1}{e^2 R_1} \Delta F_1^{\pm} N_B(\Delta F_1^{\pm}), \tag{A1}$$

where $N_B(\omega) = 1/[\exp(\omega/T) - 1]$ is the Bose function and R_1 is the tunneling bare resistance. A similar expression can be written for the discharge process through the second tunnel barrier by changing the index "1" to "2." Here $\Delta F_1^{\pm}$ is the change of effective free energy between the initial and the final states:

$$\Delta F_1^{\pm} = \frac{e^2}{C_\Sigma}\left\{\frac{1}{2} \pm \left(n - \frac{Q_s}{e}\right) \pm \frac{(C_2 + C_g/2)V}{e}\right\}, \tag{A2a}$$

$$\Delta F_2^{\pm} = \frac{e^2}{C_\Sigma}\left\{\frac{1}{2} \pm \left(n - \frac{Q_s}{e}\right) \mp \frac{(C_1 + C_g/2)V}{e}\right\}, \tag{A2b}$$

where

$$Q_s = Q_0 + \sum_i \int_i d\mathbf{n}_i \cdot \mathbf{P}_i. \tag{A3}$$

In the orthodox theory, $Q_s = Q_0$. For "slow" ferroelectric we have $\int_i d\mathbf{n}_i \cdot \mathbf{P}_i = q_{\rm fe} = q_1^0 \tanh(\frac{\langle\phi\rangle + \frac{V}{2}}{V_s}) + q_2^0 \tanh(\frac{\langle\phi\rangle - \frac{V}{2}}{V_s})$, while for "fast" we find $\int_i d\mathbf{n}_i \cdot \mathbf{P}_i = q_1^0 \tanh(\frac{\phi(n) + \frac{V}{2}}{V_s}) + q_2^0 \tanh(\frac{\phi(n) - \frac{V}{2}}{V_s})$. The $\Gamma_{n\to n+1}$ rates in the detailed-balance relations (2) are defined as follows:

$$\Gamma_{n\to n+1} \equiv \Gamma^{(1)}_{n\to n+1} + \Gamma^{(2)}_{n\to n+1}, \tag{A4a}$$

$$\Gamma_{n\to n-1} \equiv \Gamma^{(1)}_{n\to n-1} + \Gamma^{(2)}_{n\to n-1}. \tag{A4b}$$

2. Approximation near the "degeneracy point"

The probabilities near the degeneracy point $Q_0 = 1/2$ can be found using the orthodox theory

$$p(0) = \frac{\Gamma_{1\to 0}}{\Gamma_{0\to 1} + \Gamma_{1\to 0}}, \quad p(1) = \frac{\Gamma_{0\to 1}}{\Gamma_{0\to 1} + \Gamma_{1\to 0}}. \tag{A5}$$

Here Eq. (A2) reduces to

$$\Delta F_1^{+}(0) = -2\frac{E_c}{e}\left[\delta Q_s - \left(C_2 + \frac{C_g}{2}\right)V\right], \tag{A6}$$

$$\Delta F_2^{+}(0) = -2\frac{E_c}{e}\left[\delta Q_s + \left(C_1 + \frac{C_g}{2}\right)V\right], \tag{A7}$$

where $\delta Q_s = \delta Q_0 + \sum_i \int_i d\mathbf{n}_i \cdot \mathbf{P}_i$ and $\delta Q_0 = Q_0 - e/2$. Here $\Delta F_1^{+}(0) = -\Delta F_1^{-}(1)$ and $\Delta F_2^{+}(0) = -\Delta F_2^{-}(1)$.

Using Eqs. (A4) and (A5) we find $p(1)^{-1} = 1 + \exp[2E_c(\delta Q_0 + q_{\rm fe})/eT]$. Finally, using Eq. (5) we obtain Eq. (8).

3. Hysteresis width

The criterion for conductivity hysteresis in Eq. (10) can be derived using Eq. (8) for an average potential. This equation has three solutions if the slope, derivative of $\langle\phi\rangle$, of the function in the right-hand side is larger than the slope of the linear dependence in the left-hand side.

The estimate of the hysteresis width ΔQ can be done using the following assumptions: (1) the polarization is linearly depend on the average potential $q_{\rm fe}(\langle\phi\rangle) \approx q_0/V_s$; (2) we replace the hyperbolic tangents by the piecewise straight function $Z(x) = 1$ if $|x| > 1$ and $Z(x) = x$ if $|x| < 1$; and (3) we neglect the slow function $2q_{\rm fe}(\langle\phi\rangle)/e$ in the right-hand side.

For $E_c/T \gg 1$ the criterion of the conductivity hysteresis, Eq. (10), can be obtained using the formula for hysteresis width considering $\Delta Q > 0$.

---

[1] M. Dawber, I. Szafraniak, M. Alexe, and J. Scott, J. Phys. C **15**, L667 (2003).
[2] C. Ahn, K. Rabe, and J.-M. Triscone, Science **303**, 488 (2004).
[3] M. Dawber, K. M. Rabe, and J. F. Scott, Rev. Mod. Phys. **77**, 1083 (2005).
[4] L. Wang, J. Yu, Y. Wang, G. Peng, F. Liu, and J. Gao, J. Appl. Phys. **101**, 104505 (2007).
[5] Y.-J. Zhang, T.-L. Ren, and L.-T. Liu, Integrated Ferroelectrics **95**, 199 (2007).
[6] J. F. Scott, Science **315**, 954 (2007).
[7] P. Maksymovych, S. Jesse, P. Yu, R. Ramesh, A. P. Baddorf, and S. V. Kalinin, Science **324**, 1421 (2009).
[8] Y.-H. Chu, L. W. Martin, M. B. Holcomb, M. Gajek, S.-J. Han, Q. He, N. Balke, C.-H. Yang, D. Lee, W. Hu, Q. Zhan, P.-L. Yang, A. Fraile-Rodriguez, A. Scholl, S. X. Wang, and R. Ramesh, Nat. Mater. **7**, 478 (2008).
[9] W. Lee, H. Han, A. Lotnyk, M. A. Schubert, S. Senz, M. Alexe, D. Hesse, S. Baik, and U. Gösele, Nat. Nanotechnol. **3**, 402 (2008).
[10] S. V. Kalinin, A. N. Morozovska, L. Q. Chen, and B. J. Rodriguez, Rep. Prog. Phys. **73**, 056502 (2010).
[11] J. Sinsheimer, S. J. Callori, B. Bein, Y. Benkara, J. Daley, J. Coraor, D. Su, P. W. Stephens, and M. Dawber, Phys. Rev. Lett. **109**, 167601 (2012).
[12] S. J. Callori, J. Gabel, D. Su, J. Sinsheimer, M. V. Fernandez-Serra, and M. Dawber, Phys. Rev. Lett. **109**, 067601 (2012).
[13] N. Ortega, A. Kumar, J. Scott, D. B. Chrisey, M. Tomazawa, S. Kumari, D. Diestra, and R. Katiyar, J. Phys. C **24**, 445901 (2012).
[14] A. Chanthbouala, V. Garcia, R. O. Cherifi, K. Bouzehouane, S. Fusil, X. Moya, S. Xavier, H. Yamada, C. Deranlot, N. D. Mathur, M. Bibes, A. Barthélémy, and J. Grollier, Nat. Mater. **11**, 860 (2012).
[15] M. Y. Zhuravlev, S. Maekawa, and E. Y. Tsymbal, Phys. Rev. B **81**, 104419 (2010).
[16] L. Landau, E. Lifshitz, and L. Pitaevskii, Electrodynamics of Continuous Media (Elsevier, Oxford, 2004), Vol. 8.
[17] A. Gruverman, O. Auciello, and H. Tokumoto, Annu. Rev. Mater. Sci. **28**, 101 (1998).
[18] S. Jesse, P. Maksymovych, and S. V. Kalinin, Appl. Phys. Lett. **93**, 112903 (2008).
[19] B. Rodriguez, X. Gao, L. Liu, W. Lee, I. Naumov, A. Bratkovsky, D. Hesse, and M. Alexe, Nano Lett. **9**, 1127 (2009).
[20] D. Averin and K. Likharev, Mesoscopic Phenomena Solids **30**, 173 (1991).
[21] D. V. Averin, A. N. Korotkov, and K. K. Likharev, Phys. Rev. B **44**, 6199 (1991).
[22] M. Devoret and H. Grabert, *Single Charge Tunneling* (Plenum, New York, 1992), Vol. 264.
[23] C. Wasshuber, *Computational Single-Electronics* (Springer, Berlin, 2001).
[24] A. Glatz, N. M. Chtchelkatchev, and I. S. Beloborodov, Phys. Rev. B **86**, 045440 (2012).
[25] N. M. Chtchelkatchev, A. Glatz, and I. S. Beloborodov, J. Phys. C **25**, 185301 (2013).
[26] N. M. Chtchelkatchev, A. Glatz, and I. S. Beloborodov, Phys. Rev. B **88**, 125130 (2013).
[27] S. Kafanov and N. M. Chtchelkatchev, J. Appl. Phys. **114**, 073907 (2013).
[28] Y.-K. Yoon, D. Kim, M. G. Allen, J. S. Kenney, and A. T. Hunt, IEEE Trans. Microwave Theory Techniques **51**, 2568 (2003).
[29] M. Vainberg and V. Trenogin, *Theory of Branching of Solutions of Non-linear Equations* (Wolters-Noordhoff B. V., Groningen, 1974).
[30] F. De Guerville, I. Luk'yanchuk, L. Lahoche, and M. El Marssi, Mater. Sci. Eng. B **120**, 16 (2005).
[31] B. A. Strukov and A. P. Levanyuk, *Ferroelectric Phenomena in Crystals* (Springer, Geidelberg, 1998).
[32] O. G. Udalov, N. M. Chtchelkatchev, A. Glatz, and I. S. Beloborodov, Phys. Rev. B **89**, 054203 (2014).
[33] P. C. Joshi and S. B. Krupanidhi, Appl. Phys. Lett. **62**, 1928 (1993).
[34] P. K. Larsen, G. L. M. Kampschoer, M. J. E. Ulenaers, G. A. C. M. Spierings, and R. Cuppens, Appl. Phys. Lett. **59**, 611 (1991).
[35] X. S. Wang, Z. C. Wu, J. F. Webb, and Z. G. Liu, Appl. Phys. A **77**, 561 (2003).
[36] C.-S. Tu, R. R. Chien, C.-M. Hung, V. H. Schmidt, F.-T. Wang, and C.-T. Tseng, Phys. Rev. B **75**, 212101 (2007).
[37] C.-S. Tu, C.-L. Tsai, J.-S. Chen, and V. H. Schmidt, Phys. Rev. B **65**, 104113 (2002).
[38] H. Hu and S. B. Krupanidhi, J. Appl. Phys. **74**, 3373 (1993).
[39] V. M. Fridkin, Phys. Usp. **49**, 193 (2006).
[40] J. Junquera and P. Ghosez, Nature (London) **422**, 506 (2003).
[41] Q. Zhang, H. Xu, F. Fang, Z.-Y. Cheng, F. Xia, and H. You, J. Appl. Phys. **89**, 2613 (2001).